Investigation of the itinerant metamagnetic system Hf0.75Ta0.25Fe2 under extreme conditions of pressure or magnetic field

L. V. B. Diop, O. Prokhnenko, O. Isnard, Géraldine Ballon, J.P. Itié

Investigation of the itinerant metamagnetic system $Hf_{0.75}Ta_{0.25}Fe_2$ under extreme conditions of pressure or magnetic field

L. V. B. Diop[1†], O Prokhnenko[2], O Isnard[3], G Ballon[4], J P Itié[5]

[1]Université de Lorraine, CNRS, IJL, F-54000 Nancy, France
[2]Helmholtz-Zentrum Berlin für Materialien und Energie, Hahn-Meitner-Platz 1, D-14109 Berlin, Germany
[3]Université Grenoble Alpes, CNRS, Institut NEEL, BP166x, F-38042 Grenoble cedex 9, France
[4]Laboratoire National des Champs Magnétiques Intenses (UPR 3228, CNRS-UPS-UGA-INSA), F-31400 Toulouse Cedex, France
[5]Synchrotron SOLEIL, L'Orme Merisiers St Aubin BP48, F-91192 Gif Sur Yvette, France

The magnetic and structural properties of $Hf_{0.75}Ta_{0.25}Fe_2$ have been investigated under the duplicate conditions, i.e., high magnetic fields and high pressures, by combining magnetization measurements up to 26 T, neutron powder diffraction experiments up to 14.5 T, and angle dispersive synchrotron x-ray diffraction up to 10 GPa. The intermetallic compound $Hf_{0.75}Ta_{0.25}Fe_2$ exhibits an antiferromagnetic (AFM) ground state below the Néel temperature T_N = 342 K. In the AFM structure, the Fe-6h magnetic moments (1.02 μ_B at 2 K) align along the *c* axis while Fe atoms at 2a sites are not magnetically ordered. We further show that the AFM ground state gets transformed into a ferromagnetic (FM) state via a field-induced metamagnetic phase transition. Magnetic-field dependent neutron diffractograms demonstrate that FM phase sets in with a change of the easy magnetization direction from axial to basal-plane and an extremely anisotropic lattice expansion. The unit cell expands drastically in the basal plane upon increasing the applied magnetic field, while its dimension along *c*-axis shrinks slightly; resulting in a huge positive volume magnetostriction $\Delta V/V$ = 0.78 %. The application of hydrostatic pressure leads to the continuous decrease of the cell parameters. The shrinkage of the hexagonal cell is anisotropic with a larger compression along the six-fold symmetry axis *c*. A bulk modulus of K_0 = 247 GPa has been deduced from the pressure-volume relationship.

Keywords: neutron powder diffraction, spin reorientation, volume magnetostriction, spin fluctuations

† leopold.diop@univ-lorraine.fr;

1. Introduction

The itinerant electron metamagnetism (IEM), i.e., field-induced first-order transition from a low magnetic moment state to a high magnetic moment state, is an essential physical phenomenon, describing magnetic properties of intermetallic compounds, demonstrating technologically important giant magnetocaloric, magnetoelastic and magnetoresistive effects [1-4]. The discovery of giant magnetocaloric effect in the itinerant metamagnetic system $La(Fe,Si)_{13}$ [1], has opened new perspectives for room temperature magnetic refrigeration. This has triggered a spectacular upsurge of interest in magnetic cooling and the development of many researches from the viewpoints of both fundamental physics and technological applications.

One interesting example of IEM system is the Laves phase compounds $Hf_{1-x}Ta_xFe_2$. In the whole concentration range of x, the pseudo-binary system $Hf_{1-x}Ta_xFe_2$ adopts the hexagonal $MgZn_2$-type structure (C-14 Laves phase, space group $P6_3/mmc$). There are two inequivalent positions for Fe atoms, 2a and 6h, and one position, 4f for Hf/Ta atoms in this structure. The magnetic ground state changes at a Ta concentration of about $x = 0.25$ from ferromagnetic (FM) for Hf rich to antiferromagnetic (AFM) for Ta rich side . In the intermediate concentration range $0.1 < x < 0.25$, the alloys exhibit temperature-induced magnetic transitions from ferromagnetic (FM) to antiferromagnetic (AFM) order and then to the paramagnetic (PM) state upon heating [5-13]. In the FM ground state, the magnetism comes from Fe atoms on the two crystallographically inequivalent sites, 2a and 6h, both carrying a sizable magnetic moment. The high-temperature AFM phase has a complex spin configuration with two independent Fe sublattices: only 3/4 of the Fe atoms are involved in the AFM arrangement, namely those located on 6h crystal sites, whereas Fe atoms occupying 2a Wyckoff positions carry no ordered magnetic moment [5,8,10,13,20]. The FM-AFM magnetic transition is of first order and is accompanied by an isomorphic (without change of symmetry) lattice collapse, large magnetocaloric [14-16], magnetoresistive [6,10] and magnetovolume effects [6,12,17-19] as well as a giant negative thermal expansion [8,9,11]. Staircase-like transitions and anomalous thermomagnetic irreversibility arising due to kinetic arrest have also been observed in $Hf_{1-x}Ta_xFe_2$ compounds (x = 0.225, 0.230, and 0.235) [21-23]. Interestingly, peculiar and unconventional thermal effects across the FM-AFM first-order transition were most recently discovered in $Hf_{0.82}Ta_{0.18}Fe_2$ [7]. Such thermal effects result in warming (cooling) when heat is extracted from (supplied to) the material, thus providing indisputable evidence of metastable superheated FM and supercooled AFM states [7]. Changes from ferromagnetism to antiferromagnetism can be induced by external pressure; for instance, ferromagnetic

$Hf_{0.825}Ta_{0.175}Fe_2$ becomes AFM at pressures beyond 0.75 GPa (critical pressure) that corresponds to the decrease of volume of only 0.5% [6]. An investigation of the interatomic Fe–Fe exchange coupling coefficients and their lattice dependence demonstrated that the ferromagnetic interaction with the first shell is remarkably reduced upon shrinkage of the *a* cell parameter [19]. Another fascinating result of the theoretical calculations in Ref. [19] is that the Fe6h–Fe6h coupling is always positive meaning that these interactions will favour a ferromagnetic spin configuration within the atomic plane containing the Fe6h positions with Fe6h as near neighbours. The magnetic phase diagram of this pseudo-binary compounds $Hf_{1-x}Ta_xFe_2$ ($0.1 < x < 0.25$) has been qualitatively explained on the basis of the spin fluctuations theory of itinerant-electron system developed by Moriya and Usami (M–U) [24].

Up to now, the extensive investigations devoted to the $Hf_{1-x}Ta_xFe_2$ compounds have mainly focused on the intermediate composition range $0.1 < x < 0.25$. It appears there have been no direct measurements of the magnetic structure of the compounds with $x \geq 0.25$, that is, the precise magnetic structure of the AFM ground state remains an open question.

The present work aims at answering the open questions on the basis of an experimental study carried out on purposefully produced compound of composition $Hf_{0.75}Ta_{0.25}Fe_2$. To determine the magnetic structures and understand their coupling with the lattice, we conducted a detailed neutron powder diffraction study as a function of both temperature and applied magnetic field. In addition, a careful look at the literature data led us to notice that despite the extensive investigations noted above, there appears to have been no experimental works addressing the high-pressure behaviour of the crystallographic sublattice in the series of compounds $(Hf,Ta)Fe_2$. To contribute to the understanding of the role of volume in the pseudo-binary system $(Hf,Ta)Fe_2$, we have investigated the effect of hydrostatic pressure (up to 10 GPa) on the structural properties of $Hf_{0.75}Ta_{0.25}Fe_2$ by means of high-resolution synchrotron x-ray diffraction.

2. Experimental methods

The polycrystalline alloy of composition $Hf_{0.75}Ta_{0.25}Fe_2$ was synthetized by arc melting high-purity constituting metals (at least 99.95%) under a purified argon gas atmosphere. The sample was melted several times with the button flipped over after each melting, which is usually sufficient to achieve compositional homogeneity. The so-obtained ingot was wrapped in tantalum foil, sealed in an evacuated quartz tube and subsequently annealed in a resistive furnace as follows. It was heated up to 1273 K at a rate of 5 K/minute and kept at this temperature for 7 days. Then, the power was switched off and the furnace quickly cooled down

to room temperature. The room temperature crystal structure and phase purity of the synthetized material was checked by standard x-ray powder diffraction using a Siemens D5000 diffractometer in reflection mode with the Bragg–Brentano geometry and Co-Kα radiation.

Magnetization curves were measured in steady magnetic fields up to 10.5 T at temperatures ranging from 2 K to 500 K using extraction-type magnetometers [25]. The magnetization measurements were extended up to 26 T using a non-destructive pulsed-field magnet at the French National High Magnetic Field Laboratory (LNCMI) in Toulouse. A single 1.25 MJ capacitor bank was employed. When fully charged, this could produce a maximum field of 53 T with a rise time of about 25 ms and a total pulse duration of 150 ms. In our measurements the capacitor module was charged to about one-half. A detailed description of the pulsed-field facility can be found in Ref. [26]. All pulsed-field data were calibrated against the magnetization recorded in steady magnetic fields.

Neutron powder diffraction (NPD) experiments were performed at the Institut Laue Langevin (ILL) in Grenoble, France. About 3 g of fine powder were introduced into a cylindrical vanadium container (D = 6 mm, H = 5 cm) and mounted on the stick of a He cryostat, whose contribution to the diffraction patterns was eliminated using a radial oscillating collimator. Several diffractograms were collected at selected temperatures ranging between 2 and 375 K on the high-intensity two-axis powder diffractometer D1B with a detector angular range coverage $5° \leq 2\theta \leq 128°$ which is especially suited for magnetic structure determination. The data were collected using a ^{3}He multicounter containing 1280 detection cells with a step of 0.1° between neighbouring cells. A neutron incident wavelength of 2.52 Å was selected by a (002) Bragg reflection of a pyrolytic graphite monochromator, the take-off angle being 44.2° in 2θ. All measurements were performed upon heating after a stabilization time of 3 minutes with typical acquisition times of 20 minutes per isotherm. Due to the high flux available on the instrument, a second set of diffraction patterns was recorded *in situ* every 3.5 K while ramping the temperature from 2 K to 300 K. Rietveld analysis of the collected data was done using the FullProf suite software package [27], which allows the simultaneous refinement of structural and magnetic profiles.

High-field neutron diffraction experiments were carried out on the Extreme Environment Diffractometer (EXED) at the BER II research reactor at Helmholtz-Zentrum Berlin, Germany. Neutron measurements under applied magnetic fields of up to 14.5 T (superconducting magnet) were performed on pelletized sample, to avoid reorientation of the crystallites. For neutron detection, the time-of-flight (TOF) instrument EXED is equipped with

1/2” diameter position-sensitive ^{3}He detector tubes (GE Reuter Stokes). These tubes are combined into 4 detector banks (48 tubes/bank) that can be positioned at different angles and distances around the sample environment [28-29]. Our diffraction experiments using EXED focused on the low angle (large *d* spacing) region with the aim to concentrate on the magnetic signal.

Angle-dispersive x-ray powder diffraction data under hydrostatic pressures of up to 10 GPa were obtained using gasketed diamond anvil cells (DAC) at the PSICHÉ beamline (monochromatic radiation $\lambda = 0.3738$ Å) of the French Synchrotron facility (SOLEIL), at room temperature. The powder sample is loaded into the gasket hole along with small chips of ruby. A mixture of methanol and ethanol was employed as a pressure-transmitting medium. Accurate determination of sample pressure was made by the ruby fluorescence method. In order to improve the powder statistic, the sample was rotated ±5° during the exposure. The sample-to-detector distance was calibrated using a polycrystalline powder CeO_2 standard. Two-dimensional diffraction images were recorded by means of a MAR detector and the resulting diffraction data were azimuthally integrated with the FIT2D program [30], yielding one dimensional intensity versus diffraction angle 2θ patterns. A precise determination of the unit-cell parameters was obtained by a least-squares refinement of the diffraction patterns, including all the observed Bragg reflections.

3. Results and discussion

3.1. Magnetic susceptibility and magnetization

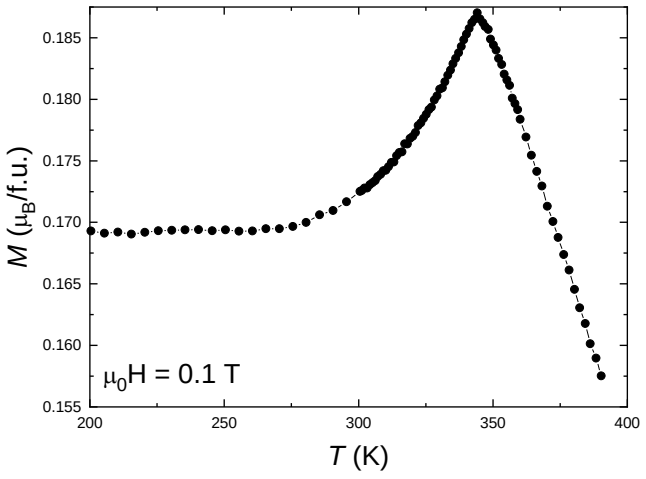

Figure 1. Temperature dependence of the magnetization for $Hf_{0.75}Ta_{0.25}Fe_2$.

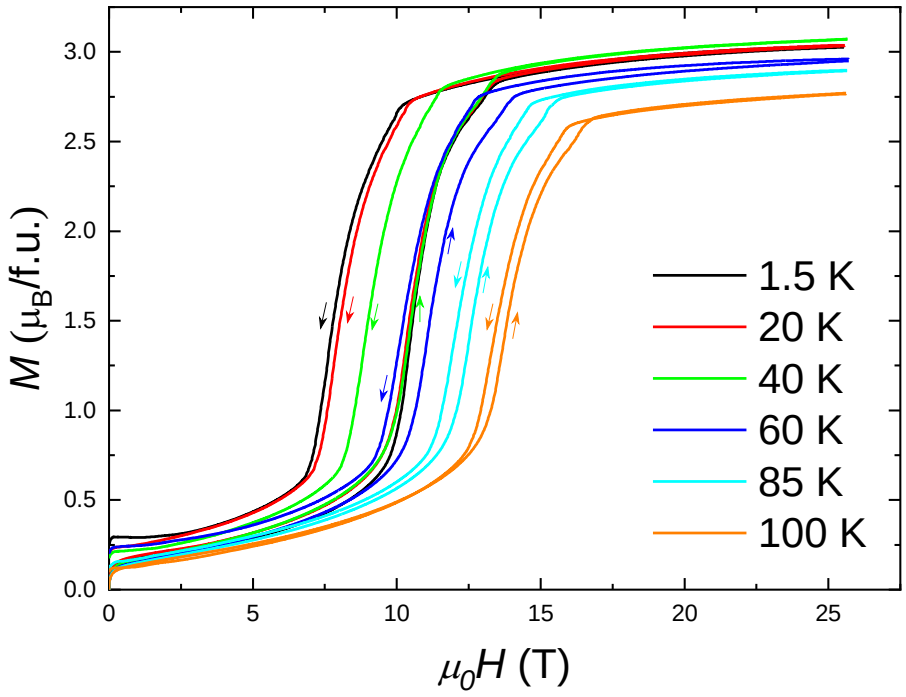

Figure 2. Magnetization curves of $Hf_{0.75}Ta_{0.25}Fe_2$ measured between 1.5 and 100 K in pulsed fields.

Figure 1 presents the thermomagnetic curve, *M(T)*, of the zero-field cooled (ZFC) sample, recorded upon heating in an applied magnetic field of 0.1 T. The peak at 342 K in the isofield magnetization curve of $Hf_{0.75}Ta_{0.25}Fe_2$ corresponds to the Néel temperature T_N reflecting the transition from an AFM state to a PM phase. Field-dependent magnetization curves *M(H)*, at several fixed temperatures ranging from 1.5 to 100 K, are displayed in Figure 2 for the thermally demagnetized $Hf_{0.75}Ta_{0.25}Fe_2$ sample. For the sake of clarity, just a selection of curves is shown in Figure 2 but all of the measured magnetization data were employed to plot the temperature dependence of the critical field illustrated in Figure 3. The *M(H)* curves exhibit an interesting field-induced metamagnetic phase transition between the AFM and FM states. The metamagnetic phase transformation proceeds through a progressive conversion of the AFM phase into FM domains with increasing the applied magnetic field. At 1.5 K, the field-induced metamagnetic phase transition is remarkable in two ways: (i) by the huge magnetization change and (ii) by the presence of a particularly large magnetic hysteresis of 3 T. One remarks that, when the external magnetic field is reduced to zero, the system recovers the initial state; this indicates that the forced FM phase loses its stability when the applied field is brought back to zero. In the investigated temperature interval 1.5 – 100 K, we observed a clear hysteresis against the field scan, which is characteristic of the first-order nature of the phase transition. The width of the magnetic hysteresis becomes smaller upon heating. The

saturation magnetization M_{sat} of the field-induced FM phase amounts to 3.02 μ_B/f.u. at 1.5 K; leading to an average magnetic moment of 1.51 μ_B per Fe atom. The saturation magnetization of the forced FM state of our sample $Hf_{0.75}Ta_{0.25}Fe_2$ compares very well with the value of the spontaneous magnetization M_S = 3.10 μ_B/f.u. obtained at 4 K for the ferromagnetic parent compound $HfFe_2$ [6].

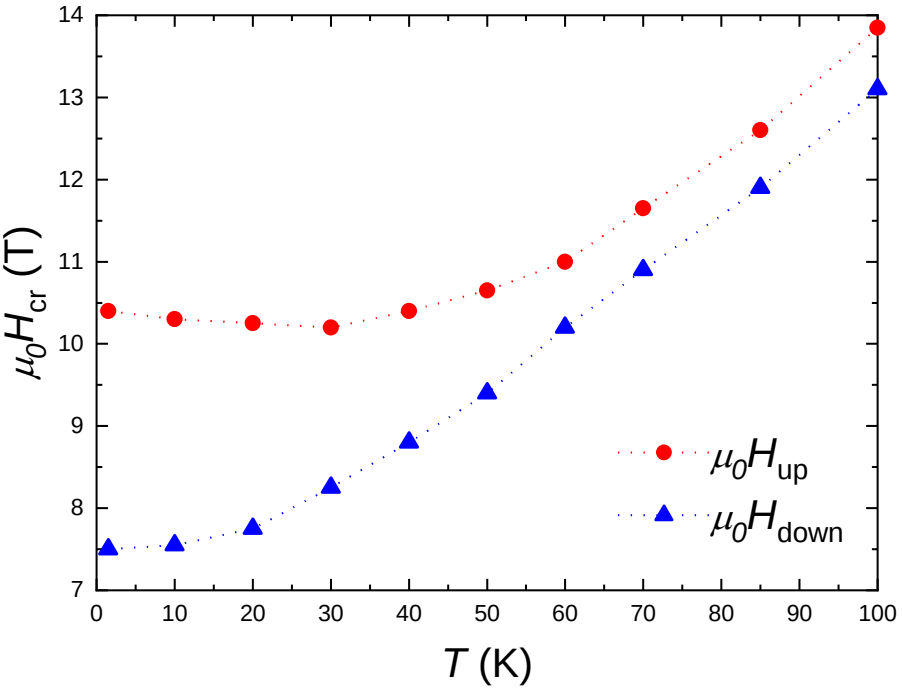

Figure 3. Thermal evolution of the critical field $\mu_0 H_{cr}$ upon increasing (up) or decreasing (down) the applied magnetic field for $Hf_{0.75}Ta_{0.25}Fe_2$.

The critical field, $\mu_0 H_{cr}$, of the AFM-FM metamagnetic transition is deduced from the peak position of the derivative of the *M(H)* curves and the corresponding values are plotted against temperature in Figure 3. The value of the transition field $\mu_0 H_{cr}$ is related to the free energy difference between the AFM and FM phases. In order to overcome the energy barrier between the two magnetic phases (AFM and FM) and to accomplish the metamagnetic transformation, the application of a magnetic field beyond the transition field is required . The critical field of the field-decreasing leg of the metamagnetic phase transition, $\mu_0 H_{cr}$ (down), decreases continuously upon cooling. While the thermal variation of the transition field obtained for the field-increasing branch, $\mu_0 H_{cr}$ (up), is nonmonotonic, namely, $\mu_0 H_{cr}$ (up) decreases in the low temperature region 1.5 – 30 K, and then increases in high temperatures.

Moriya and Usami (M–U) discussed the magnetic phase transition in itinerant-electron

compounds with the competing FM and AFM phases [24]. They proposed magnetic phase diagrams in which both FM and AFM components of spin fluctuations are present. The M–U theoretical model takes into account the equilibrium state of the free energy displaying a double minimum and assumes that the thermal evolution of χ_Q/χ_0 is monotonic, where χ_0 and χ_Q represent respectively the uniform and staggered magnetic susceptibilities. In the high temperature region, the behaviour of the critical field $\mu_0 H_{cr}$ for $Hf_{0.75}Ta_{0.25}Fe_2$ which exhibits an AFM ground state is similar to that for the compounds on the intermediate composition range $0.1 < x < 0.25$ having a FM ground state (the increase of $\mu_0 H_{cr}$ upon heating being correlated to the monotonic decrease in χ_Q/χ_0). By contrast, the critical field increases with decreasing temperature at low temperatures in $Hf_{0.75}Ta_{0.25}Fe_2$ system against the M-U theoretical model. This observed behaviour indicates that the thermal variation of χ_Q/χ_0 in the low temperature region is different from that of χ_Q/χ_0 at high temperatures. The M–U theory does not take into account interactions arising from magnetovolume coupling in the free energy expansion. Consequently, we suggest that the thermal evolution of the critical field of the AFM-FM metamagnetic phase transition is explainable by considering the contribution from both the magnetic and elastic energies resulting from magnetovolume effects.

To further investigate the magnetic behaviour of Fe sublattice in the paramagnetic phase, magnetization isotherms have been measured at temperatures well above T_N. The thermal evolution of the inverse susceptibility is shown in Figure 4. The magnetic susceptibility follows Curie-Weiss law but two distinct regions are observed involving different paramagnetic Curie temperatures θ_p and Curie constants C. The determined values are summarized in Table 1. The paramagnetic susceptibility presents a break at $T^* = 400$ K. The Curie constant above T^* is found to be about 1.5 times smaller than that measured below. The effective moment μ_{eff} derived from the Curie constant is 4.25 μ_B/Fe and 3.55 μ_B/Fe below and above T^*, respectively. This study of magnetic properties of $Hf_{0.75}Ta_{0.25}Fe_2$ intermetallic in both paramagnetic and magnetically ordered states has led to remarkably different values of Fe magnetic moments in the ordered state and in the paramagnetic phase. We calculated the Rhodes-Wohlfarth ratio r for both paramagnetic domains, namely, below and above T^* and the corresponding values are listed in Table 1. The determined r values are larger than 1 and point to the itinerant character of magnetism in this compound. Following Moriya and co-workers [31-34], the observed bend at T^* of the reciprocal magnetic susceptibility of $Hf_{0.75}Ta_{0.25}Fe_2$ is due to the temperature variation of the local amplitude of spin fluctuations.

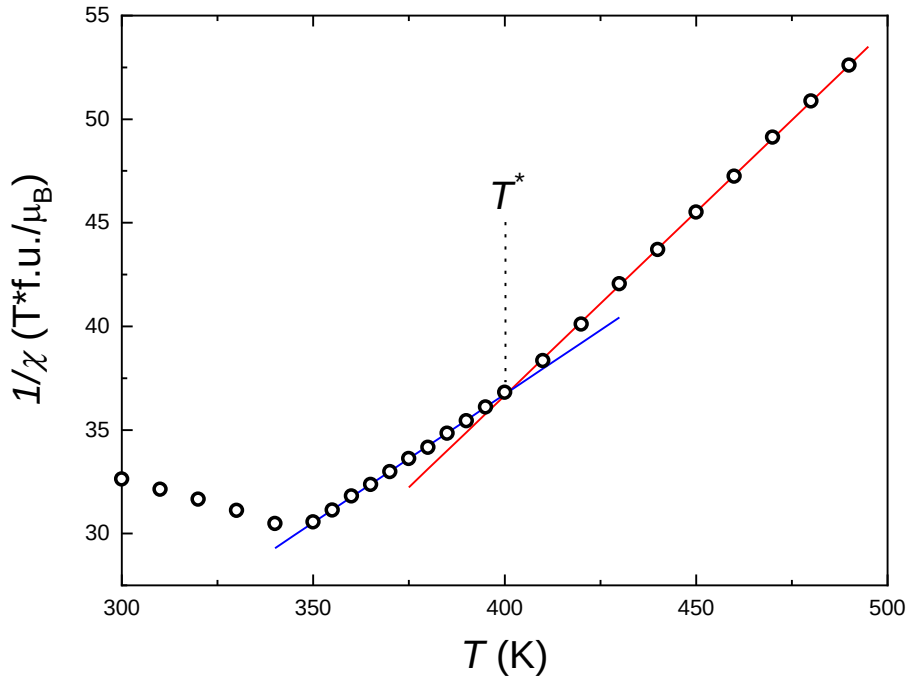

Figure 4. Thermal variation of the reciprocal magnetic susceptibility for $Hf_{0.75}Ta_{0.25}Fe_2$.

Table 1: T_N or T_C, magnetic ordering temperature; T^* temperature of change of the Curie Weiss behavior, q_s, number of carriers deduced from saturation magnetization μ_s; q_c, number of carriers deduced from Curie–Weiss constant C; μ_{eff}, paramagnetic effective moment; θ_p, paramagnetic Curie temperature and ratio $r = q_c / q_s$, for the $Hf_{0.75}Ta_{0.25}Fe_2$ compared to that of the pure Fe.

Compound	T_N/T_C (K)	μ_s 1.5 K (μ_B/Fe)	T^* (K)	q_s	C (μ_B K/f.u.T)	μ_{eff} (μ_B/Fe)	q_c	θ_p (K)	r
$Hf_{0.75}Ta_{0.75}Fe_2$	342	1.51	400	1.51	$T<T^*$ 8.08	4.25	3.37	103	2.23
					$T>T^*$ 5.64	3.55	2.69	193	1.78
α-Fe	1043	2.22	–	2.22	2.26	3.18	2.33	1093	1.05

3.2. Neutron powder diffraction (NPD)

A. Zero-field NPD measurements

In order to establish the magnetic structures of this complex system $Hf_{0.75}Ta_{0.25}Fe_2$, we have performed NPD studies. So far, no member of the (Hf,Ta)Fe_2 series of compounds with an AFM ground state has been investigated using neutron diffraction. Rietveld refinements have been performed on diffractograms recorded at selected representative temperatures in the PM and AFM states, in order to refine the crystal structure and magnetic ordering – Figures 5a and

5b. The resulting crystallographic parameters and the Fe magnetic moments deduced from the fits at 375 K and 2 K are summarized in Table 2. The diffraction pattern collected at 375 K (PM state) is characteristic of the nuclear Bragg scattering only and all the Bragg reflections could be identified to arise from the *P6₃/mmc* $MgZn_2$-type crystal structure.

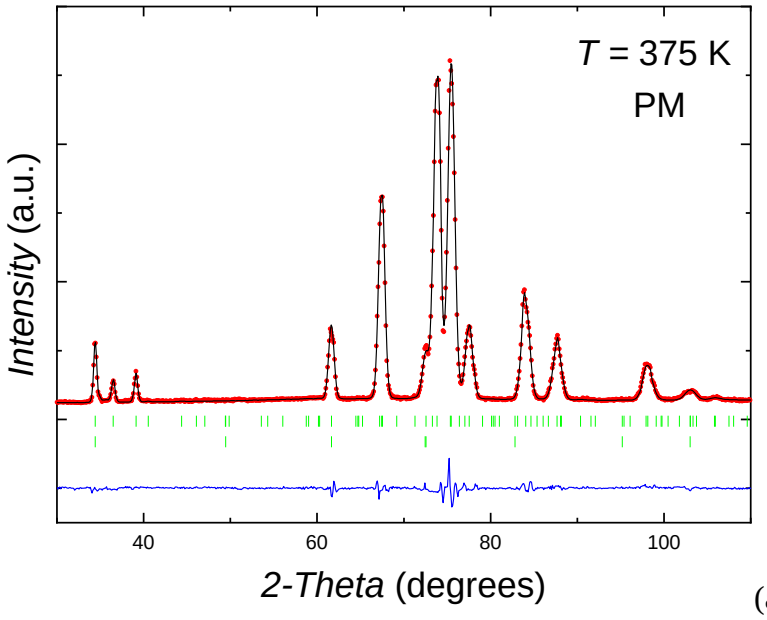

(a)

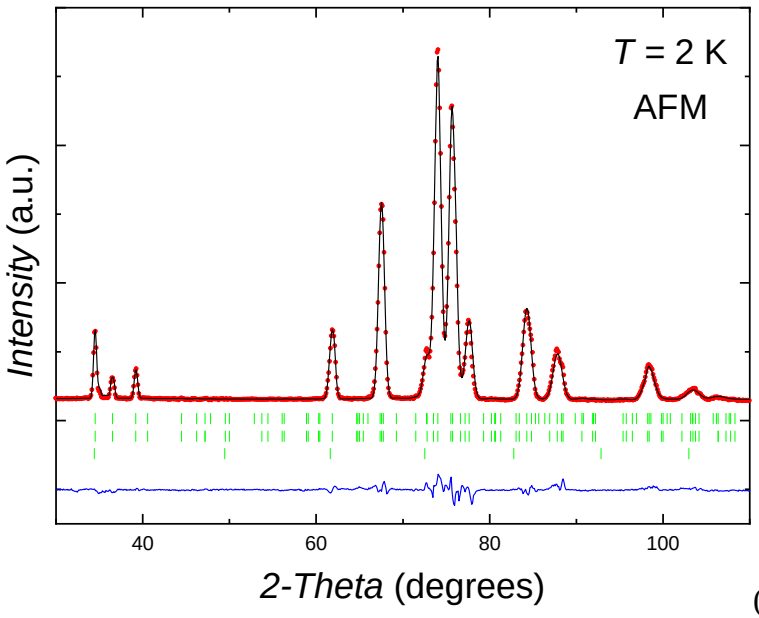

(b)

Figure 5. Refinements of the neutron diffraction patterns recorded for $Hf_{0.75}Ta_{0.25}Fe_2$ at 375 K (a) and 2 K (b). In figure (a) the top row of Bragg markers is for the $Hf_{0.75}Ta_{0.25}Fe_2$ nuclear contributions, the second row corresponds to the position of the vanadium sample environment contribution. In figure (b) the top and second rows of Bragg markers are referring to the nuclear and magnetic contributions of the $Hf_{0.75}Ta_{0.25}Fe_2$ phase. The third row is corresponding to the nuclear contribution from the vanadium sample environment.

The analysis of the NPD pattern obtained at 2 K shows that the crystallographic structure is retained at low temperature. The 2 K diffractogram presents the same Bragg peaks as the spectra collected in the PM phase. No additional magnetic reflections are detected, which implies that the corresponding AFM structure is defined by the magnetic propagation vector **k** = (0, 0, 0). In other words, the magnetic unit cell coincides with the crystallographic one. At 2 K, the best refinement is achieved for a magnetic arrangement in which Fe-6h spins align ferromagnetically within the same layer but opposite orientations on successive Fe-6h layers. In the AFM structure, the Fe magnetic moments align along the six-fold symmetry axis *c*. The refined moment for Fe-6h atoms at 2 K is 1.02 μ_B; the Fe-2a atoms are not magnetically ordered. Since the 2a Wyckoff position constitutes an inversion centre for the 6h sublattice, the molecular field acting on the 2a crystal site from the Fe-6h magnetic moments is cancelled by symmetry in this AFM spin configuration. Therefore, Fe-2a atoms display null magnetic moment. The obtained Fe magnetic moment (1.02 μ_B) is remarkably decreased in comparison with the pure Fe moment of 2.22 μ_B. This experimental result is consistent with the presence of non-magnetic Hf and Ta atoms as near neighbours. The AFM magnetic structure of $Hf_{0.75}Ta_{0.25}Fe_2$ is similar to that established elsewhere for isostructural compound $TiFe_2$ [20].

Not knowing *a priori* the orientation of the magnetic moments in the AFM ground state, Rietveld refinements of the 2 K pattern were also conducted considering an alignment of the moments in the basal-plane of the hexagonal lattice. The two principal basal-plane directions, [100] and [120], were tested. The magnetic reliability factors (R_{mag}) obtained for the two directions are very close: 14.7% and 15.3% for [100] and [120] orientation, respectively. The orientation of the magnetic moments in the basal-plane leads to much worse fits compared to that along the *c*-axis [001] which leads to much smaller reliability factor 7.11%. Consequently, at 2 K, Rietveld refinement gives a significantly better fit when the magnetic moments are along the [001] direction giving confidence to such orientation of the magnetic moments. However, it should be noted that the magnitude of the magnetic moment for Fe-6h atoms differs only very slightly between the two orientations – *c* axis and basal-plane – and Fe-2a atoms carry no ordered moment. Fitting the 2 K magnetic pattern with Fe-6h moments oriented along the *c*-axis yields the results presented in table 2.

From now on, it is clear that the magnetic structure of the AFM ground state in $Hf_{0.75}Ta_{0.25}Fe_2$ is different from the spin configuration of the high-temperature AFM phase found in compounds when $0.1 < x < 0.25$, whose ground state is the FM state. It is recalled that in the high-temperature AFM the Fe magnetic moments are confined to the basal-plane of the

hexagonal structure [13].

The thermal evolutions of the lattice parameters *a* and *c*, the *c/a* ratio, and the unit-cell volume *V* are plotted in Figures 6a, 6b, and 6c, respectively. The results of the Rietveld analysis of the thermodiffraction data reveal that the lattice constants, *a* and *c*, decrease as the temperature is lowered, thus causing the overall reduction in the unit-cell volume upon cooling. On the contrary, the *c/a* ratio decreases with increasing temperature. Below 25 K, the unit-cell parameters remain essentially constant; and then present a normal behaviour by increasing as a result of thermal expansion, with a rate of 1.03×10^{-4} Å K^{-1}, 1.56×10^{-5} Å K^{-1}, and 4.53×10^{-3} Å^3 K^{-1} for *a*, *c*, and *V*, respectively. $Hf_{0.75}Ta_{0.25}Fe_2$ intermetallic exhibit positive thermal expansion (PTE) over the investigated temperature interval. Based on the refined values of cell volume, we calculated the volumetric thermal expansion coefficient $\alpha_V = (1/V)(dV/dT)$ and a value of 26.9×10^{-6} K^{-1} is obtained at room temperature.

Table 2. Rietveld refinement results and reliability factors obtained from the analysis of the powder neutron diffraction patterns recorded at 2 K and 375 K for $Hf_{0.75}Ta_{0.25}Fe_2$.

	AFM	PM
T (K)	2 K	375
a (Å)	4.904(1)	4.925(3)
c (Å)	8.040(3)	8.045(2)
Hf /Ta (4f)		
z	0.062(1)	0.066(3)
Fe (6h)		
x	0.832(2)	0.834(3)
y = 2x	1.664(4)	1.668(6)
Fe 2a moment (μ_B)	—	—
Fe 6h moment (μ_B)	1.02(6)	—
Moment—*c*-axis angle (°)	0	—
χ^2	6.39	4.01
R_{Bragg} (%)	7.51	4.34
R_{mag} (%)	7.11	—
R_{wp} (%)	11.8	11.1
R_p (%)	12.6	11.1
R_{exp} (%)	4.69	5.52

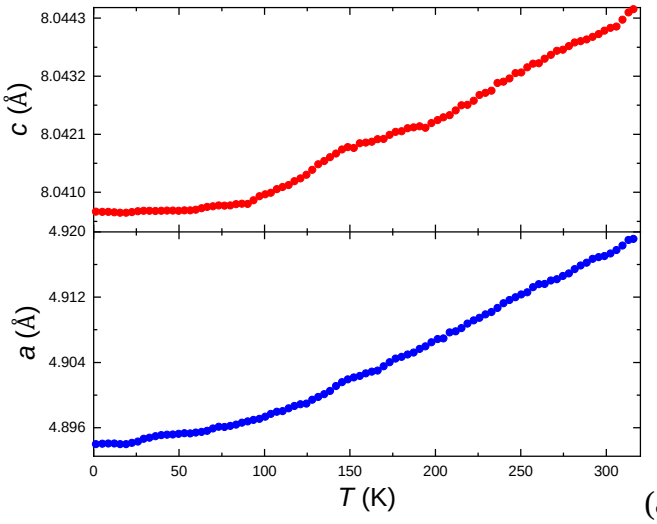

(a)

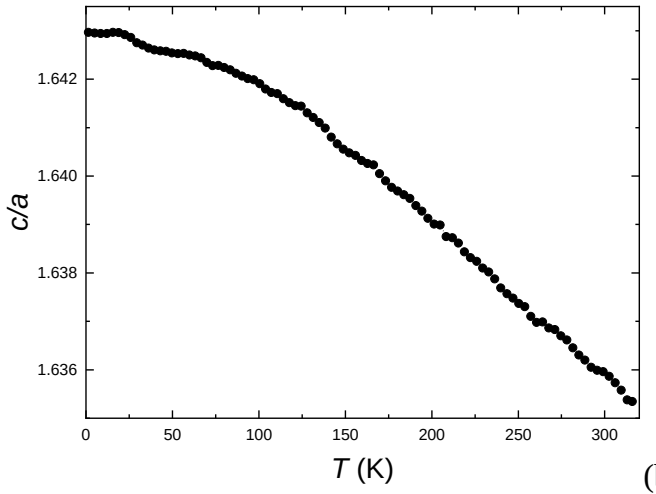

(b)

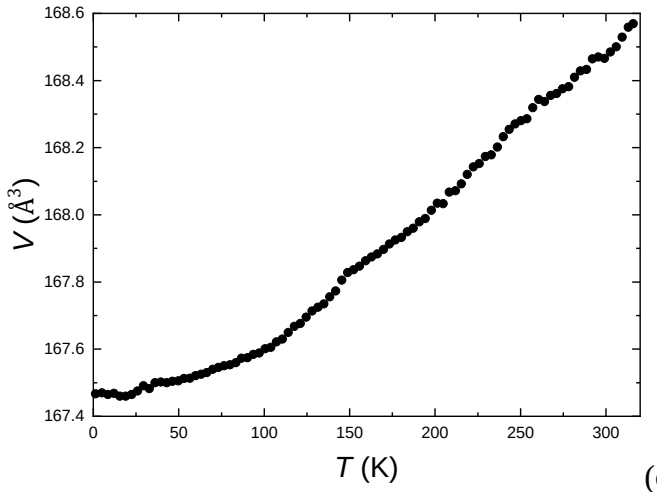

(c)

Figure 6. Thermal dependence of the lattice parameters *a* and *c* (a), *c/a* ratio (b), and unit-cell volume (c) obtained from Rietveld refinement of NPD data measured upon heating for $Hf_{0.75}Ta_{0.25}Fe_2$.

B. High-field NPD measurements

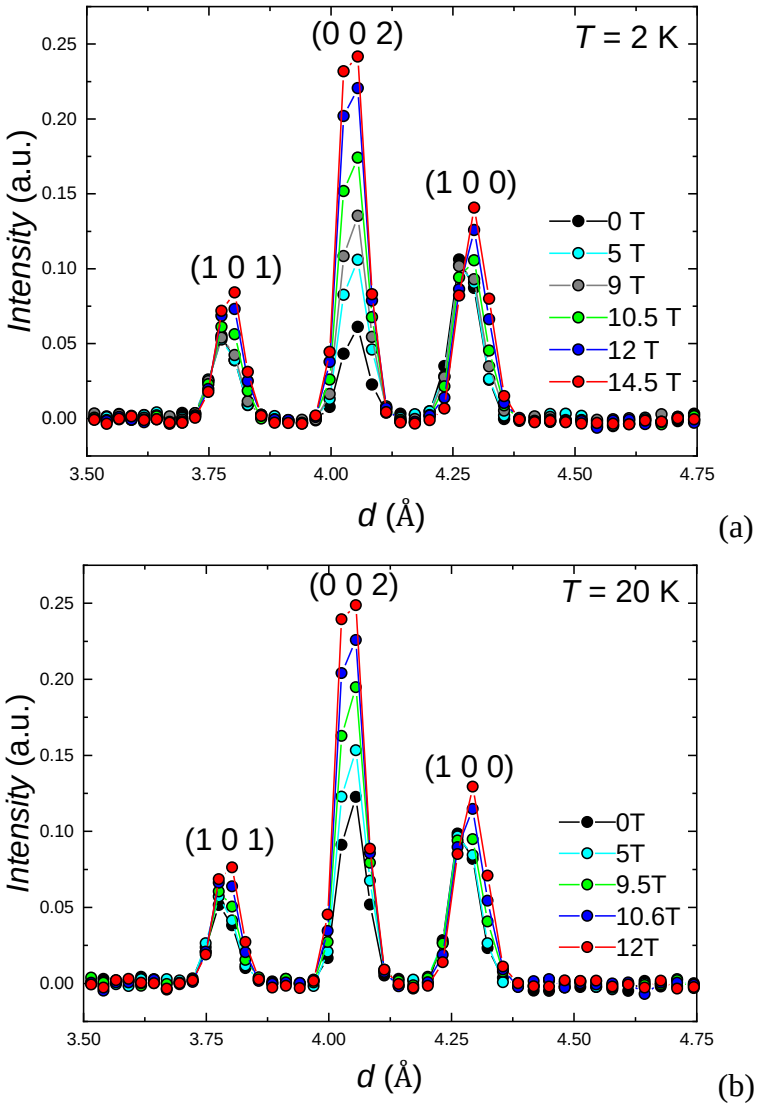

Figure 7. Normalized neutron diffractograms recorded for $Hf_{0.75}Ta_{0.25}Fe_2$ at 2 K (a) and 20 K (b) under various applied magnetic fields.

The observation of a metamagnetic phase transition by magnetization measurements prompted us to perform neutron experiments in applied magnetic field to determine the magnetic-field dependence of the structural and magnetic state of $Hf_{0.75}Ta_{0.25}Fe_2$. For this NPD experiments we used the EXED instrument in the high-intensity mode, and focused on the large *d*-spacing lines, that is, maximizing the neutrons flux for peaks displaying large *d*-spacing which appear at low diffraction angles where the generalized increase of the magnetic signal in the Bragg positions is more evident. The normalized neutron diffraction patterns at 2 K and 20 K under various applied magnetic fields are depicted in Figures 7a-7b. Our choice of these

particular temperatures is due to the fact that we aimed to observe the field-induced phase transition (see Figure 2) within the maximum available magnetic field of 14.5 T in this experiment. All the magnetic intensities are observed on top of the nuclear Bragg peaks and the contribution of the magnetic order to the NPD diagrams is reflected in the intensities of the (100), (101) and (002) reflections. It can be clearly seen on the diffraction patterns in figures 7a and 7b that there is a large difference between the spectra at zero field and under applied magnetic fields. This is most reflected in the dramatic change of intensity of the (002) peak. The intensity of the (002) line is much more susceptible to magnetic fields than that of the (100) and (101) lines. As expected the application of a magnetic field supresses the AFM phase and a FM state is induced, as can be observed in figure 7a looking especially at the diffractograms collected at 2 K at zero field and 14.5 T.

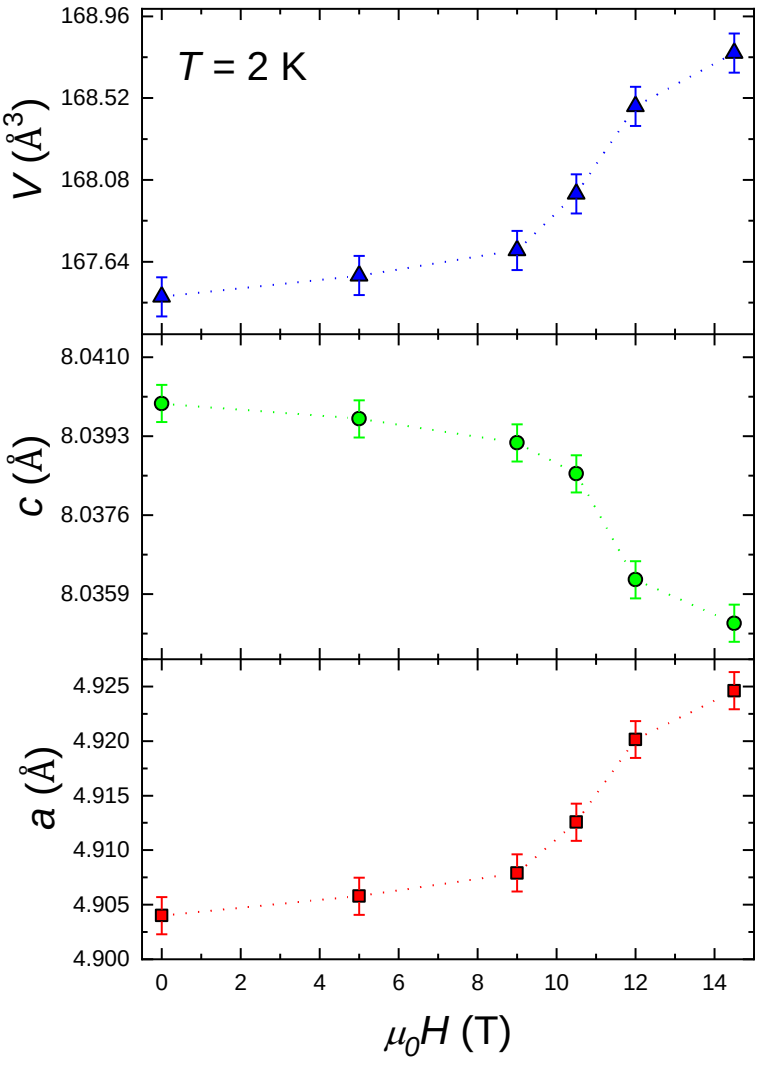

Figure 8. Unit-cell parameters of $Hf_{0.75}Ta_{0.25}Fe_2$ as a function of applied magnetic field.

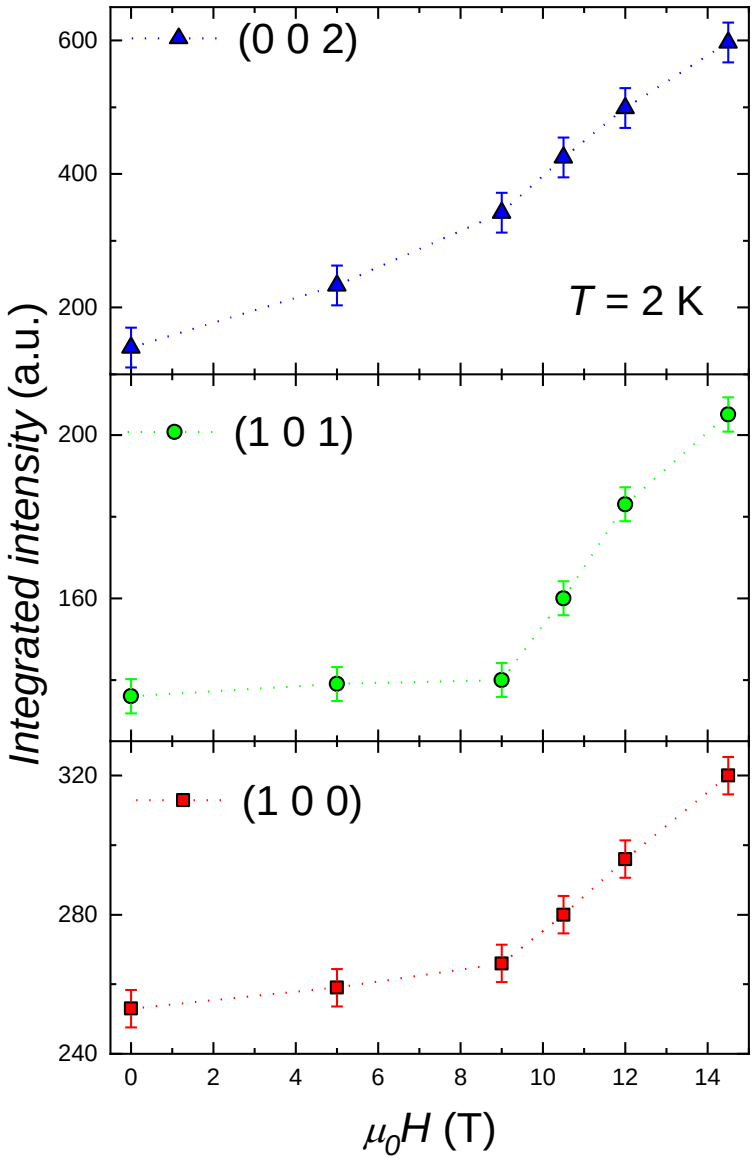

Figure 9. Integrated intensities of (100), (101) and (002) reflections at 2 K as a function of the applied magnetic field.

Although we cannot extract complete crystal structure determination from our high-field neutron data, our experiments reveal a concomitant expansion of the lattice in the basal-plane in response to the applied magnetic fields, as seen in the shift to larger *d*-spacing of the (100) and (101) Bragg peaks. The detailed magnetic field dependencies of lattice dimensions are displayed in Figure 8. One remarks a peculiarly anisotropic character of the volume expansion: the *c* lattice parameter slightly decreases with increasing the applied magnetic field, but the *a* parameter increases to a larger extent, thus causing the overall increase in the cell volume. The *a* lattice constant exhibits a large change, reaching a value of $\Delta a/a$ (2 K, 14.5 T) = 0.42 %. A tiny drop in the *c* cell parameter is observed at the magnetic transition, being smaller for the

FM phase $\Delta c/c$ (2 K, 14.5 T) = -0.059 %. Consequently, the forced volume magnetostriction is estimated to be $\Delta V/V$ (2 K, 14.5 T) = 0.78 %. The AFM-FM metamagnetic transition is accompanied by large magnetovolume effects. Our results demonstrate that the effect of the applied field is to induce a magnetic phase transformation from a low-volume AFM state to a high-volume FM state through a first-order transition at a certain critical field. The obtained value for the field-induced volume magnetostriction compares very well with the volume change $\Delta V/V$ = 0.75 % derived from dilatometric magnetostriction measurements for isostructural compound $Hf_{0.825}Ta_{0.175}Fe_2$ [12].

We have found a different effect of the magnetic field in the intensities of the three peaks at low temperature. This is illustrated in Figure 9, where the integrated intensities of the (100), (101) and (002) reflections are displayed as a function of the magnetic field at 2 K. The difference in the influence of the applied magnetic field is remarkable. While the external applied magnetic field leads to a very fast rise of the intensity associated to the (002) peak, the intensities of the (100) and (101) lines become almost field independent below 9 T and then increase rapidly as the sample undergoes a metamagnetic transition. This phenomenon is in agreement with the macroscopic magnetic measurements, where the onset of significant change in the magnetization is found at 9.25 T. Upon application of an external magnetic field, a continuously increasing magnetic scattering is observed on (002) peak indicating that a ferromagnetic component is progressively induced in the material. The magnetic contribution to (002) reflection is proportional to the square of the in-plane magnetization component since neutrons are sensitive to the component of the magnetic moment perpendicular to the scattering vector. In the forced FM state, the presence of magnetic contribution on (002) peak reveals that the Fe moments are not aligned along the *c*-axis. One could conclude that $Hf_{0.75}Ta_{0.25}Fe_2$ features a first-order field-induced spin-reorientation transition; the easy magnetization direction changes from axial to basal-plane upon application of magnetic field.

3.3. High-Pressure synchrotron x-ray diffraction (SXRD)

To probe the effect of external pressure on the crystal structure, angle dispersive synchrotron x-ray diffraction patterns have been recorded at room temperature for various applied pressures ranging from 0 to 10 GPa. In Figure 10 we compare selected SXRD patterns during compression of the sample. SXRD diffractograms collected at various pressures reveal that the hexagonal symmetry of the atomic arrangement remains unaltered within the investigated pressure range; no indication of a structural phase transition was found up to the highest applied pressure. All the observed Bragg reflections could be identified to arise from

the original C-14 Laves phase structure (space group $P6_3/mmc$). The crystal symmetry is stable up to the highest applied pressure of 10 GPa. Analysis of the diffraction patterns shows that the diffraction peaks shift to higher angles due to the contraction of the lattice. The lattice constants (a and c), deduced from least-squares refinements, are plotted in Figure 11 as a function of applied pressure. Both cell parameters decrease continuously upon compression, and values of $da/dP = -5.90\times10^{-3}$ Å GPa^{-1} and $dc/dP = -9.51\times10^{-3}$ Å GPa^{-1} are obtained. The contraction of the hexagonal cell is anisotropic and more pronounced along the c direction. In the crystal structure, the arrangements of atoms and bonds perpendicular to c-axis direction are dense, while, along c-axis direction the atoms arrange loosely, which points out it has considerable relaxation space on compression. The pressure dependence of the unit-cell volume is illustrated in Figure 12. The experimental data were fitted to a third-order Birch-Murnaghan equation of state [35] where K_0' was fixed at 4. The fit yielded $V_0 = 168.56$ Å^3 for the zero-pressure unit-cell volume and $K_0 = 247$ GPa for the bulk modulus. For comparison purposes we note that, $TiFe_2$ and $LaFe_{12}B_6$ materials have a bulk modulus of 201 GPa [36] and 204 GPa [37], respectively. The bulk modulus of $Hf_{0.75}Ta_{0.25}Fe_2$ is ≈1.2 times larger than that of the antiferromagnetic itinerant-electron system $LaFe_{12}B_6$.

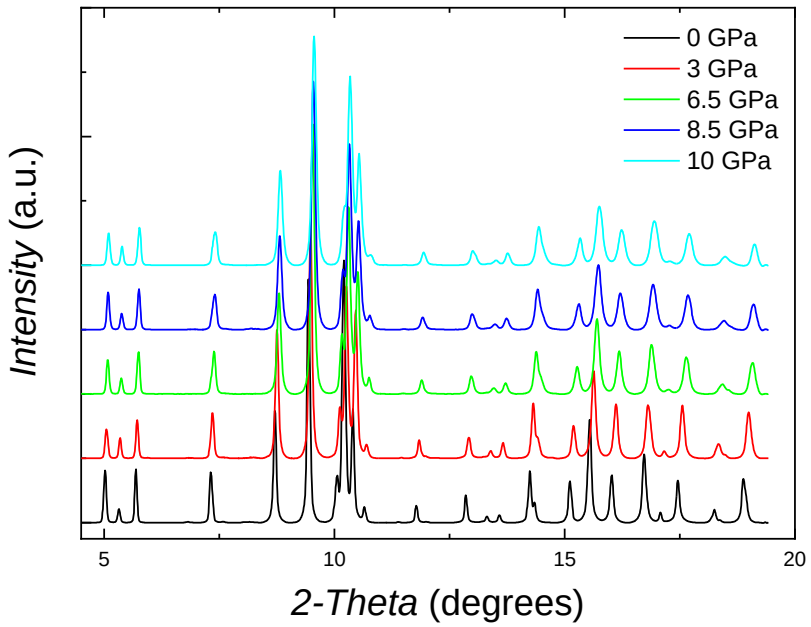

Figure 10. Synchrotron x-ray diffraction patterns collected at room temperature for $Hf_{0.75}Ta_{0.25}Fe_2$ at various applied pressures (λ = 0.3738 Å).

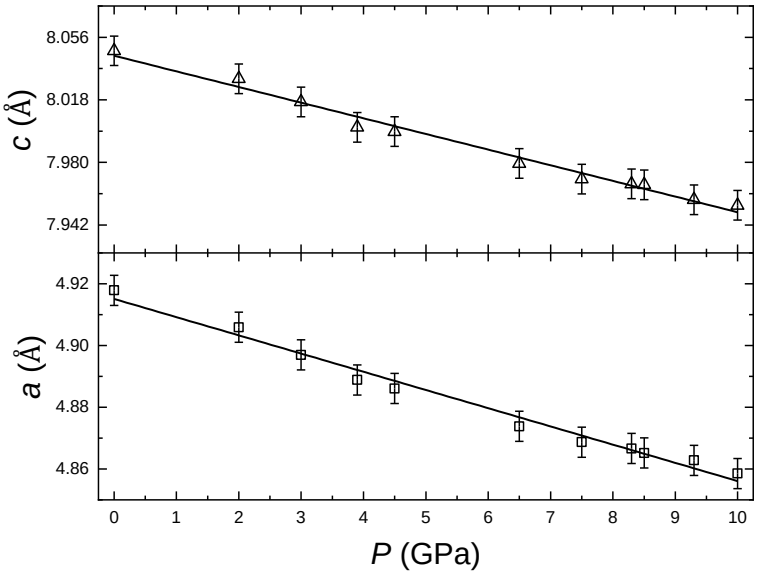

Figure 11. Lattice constants of $Hf_{0.75}Ta_{0.25}Fe_2$ as a function of applied pressure. The solid lines correspond to linear fits.

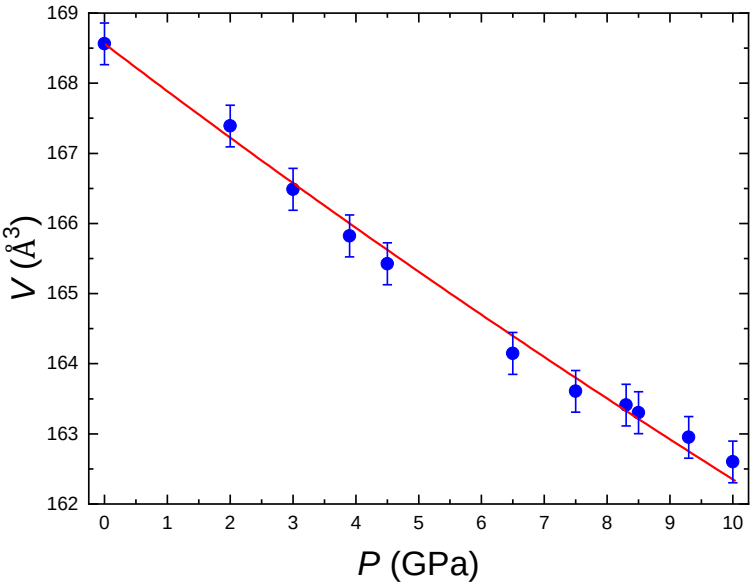

Figure 12. Unit-cell volume of $Hf_{0.75}Ta_{0.25}Fe_2$ as a function of applied pressure. The continuous red line represents the third-order Birch-Murnaghan fit for the data.

4. Conclusions

Competition between AFM and FM states in the itinerant-electron system $Hf_{0.75}Ta_{0.25}Fe_2$ has been investigated by means of neutron powder diffraction and magnetizations measurements both performed under extreme conditions of low temperature and large magnetic fields. The studied compound $Hf_{0.75}Ta_{0.25}Fe_2$ presents an antiferromagnetic order as a ground state below T_N = 342 K. The AFM ordering is only due to the Fe atoms at 6h sites which carry a magnetic moment of 1.02 μ_B at 2 K. It is demonstrated that the AFM phase

can be transformed into a FM phase via a field-induced metamagnetic transition accompanied with an in-plane lattice expansion and a change of the easy magnetization direction from axial to basal-plane. In the disordered phase, an unusual and intriguing transition from one paramagnetic state to another one involving two distinct Curie-Weiss behaviours has been observed at T^*, a critical temperature at which the reciprocal magnetic susceptibility presents a bend. Thanks to synchrotron radiation, x-ray diffraction has been carried out upon application of a high external pressure. In the investigated pressure range, no change of crystal symmetry occurs. The unit cell shrinks continuously, but in an anisotropic way with a larger compression along the high-symmetry direction *c*.

Acknowledgments

The authors gratefully acknowledge the Institut Laue Langevin and Helmholtz-Zentrum Berlin for access to the neutron facilities. We acknowledge the French Synchrotron facility SOLEIL for the allocation of beam time. We also acknowledge the support of the French National High Magnetic Field Laboratory (LNCMI), member of the European Magnetic Field Laboratory (EMFL).

References

[1] Fujita A, Fujieda S, Hasegawa Y and Fukamichi K 2003 *Phys. Rev.* B **67** 104416

[2] Yamada H and Goto T 2003 *Phys. Rev.* B **68** 184417

[3] Kozlenko D P, Burzo E, Vlaic P, Kichanov S E, Rutkauskas A V and Savenko B N 2015 Sci. Rep. **5** 8620

[4] Duc N H, Kim Anh D T and Brommer P E 2002 Physica B **319** 1.

[5] Nishihara Y and Yamaguchi Y 1983 *J. Phys. Soc. Jpn.* **52** 3630

[6] Diop L V B, Kastil J, Isnard O, Arnold Z and Kamarad J 2014 *J. Appl. Phys.* **116** 163907

[7] Bag P, Rawat R, Chaddah P, Babu P D and Siruguri V 2016 *Phys. Rev.* B **93** 014416

[8] Li B, Luo X H, Wang H, Ren W J, Yano S, Wang C W, Gardner J S, Liss K D, Miao P, Lee S H, Kamiyama T, Wu R Q, Kawakita Y and Zhang Z D 2016 *Phys. Rev.* B **93** 224405

[9] Li L F, Tong P, Zou Y M, Tong W, Jiang W B, Jiang Y, Zhang X K, Lin J C, Wang M, Yang C, Zhu X B, Song W H and Sun Y P 2018 *Acta Materialia* **161** 258

[10] Duijn H G M, Brück E, Menovsky A A, Buschow K H J, De Boer F R, Coehoorn R, Winkelmann M and Siemensmeyer K 1997 *J. Appl. Phys*. **81** 4218

[11] Li L, Tong P, Tong W, Jiang W, Ding Y, Lin H, Lin J, Yang C, Zhu F, Zhang X, Zhu X, Song W and Sun Y 2019 *Inorg. Chem.* **58** 16818

[12] Diop L V B, Amara M and Isnard O 2013 *J. Phys.: Condens. Matter* **25** 416007

[13] Diop L V B, Isnard O, Suard E and Benea D 2016 *Solid State Commun.* **229** 16

[14] Herbst J F, Furerst C D and McMichael R D 1996 *J. Appl. Phys*. **79** 5998

[15] Diop L V B, Kastil J, Isnard O, Arnold Z and Kamarad J 2015 *J. Alloys Compd.* **627** 446

[16] Han Z D, Wang D H, Huang S L, Su Z H, Tang S L and Du Y W 2004 *J. Alloys Compd.* **377** 75

[17] Morellon L, Algarabel P A, Ibarra M R, Arnold Z, and Kamarad *J 1996 J. Appl. Phys.* **80** 6911

[18] Diop L V B, Arnold Z and Isnard O 2015 *J. Magn. Magn. Mater.* **395** 251

[19] Diop L V B, Benea D, Mankovsky S and Isnard O 2015 *J. Alloys Compd.* **643** 239

[20] Rechenberg H R, Morellon L, Algarabel P A and Ibarra M R 2005 *Phys. Rev*. B **71** 104412

[21] Rawat R, Chaddah P, Bag P, Babu P D and Siruguri V 2013 *J. Phys.: Condens. Matter* **25**, 066011

[22] Bag P, Singh S, Babu P D, Siruguri V and Rawat R 2014 *Physica* B **448** 50

[23] Reddy V R, Rawat R, Gupta A, Bag P, Siruguri V and Chaddah P 2013 *J. Phys.: Condens. Matter* **25** 316005

[24] Moriya T and Usami K 1977 *Solid State Commun.* **23** 935

[25] Barlet A, Genna J C and Lethuillier P 1991 *Cryogenic* **31** 801.

[26] Portugall O, Lecouturier F, Marquez J, Givord D and Askénazy S 2001 *Physica* B **294-295** 579

[27] Rodrıguez-Carvajal J 1993 *Physica* B **192** 55

[28] Prokhnenko O, Stein W D, Bleif H J, Fromme M, Bartkowiak M and Wilpert T 2015 *Rev. Sci. Instrum.* **86** 033102

[29] Peters J, Lieutenant K, Clemens D and Mezei F 2006 *Z. Kristallogr. Suppl.* **23** 189

[30] Hammersley A P, Svensson S O, Hanfland M, Fitch A N and Hausermann D 1996 *High Press. Res.* **14** 235

[31] Moriya T 1979 *J. Magn. Magn. Mater.* **14** 1

[32] Moriya T 1991 *J. Magn. Magn. Mater*. **100** 261

[33] Kübler J, *Theory of Itinerant Electron Magnetism* (Oxford: Oxford Science Publications ISBN 0198500289, 2000)

[34] Moriya T and Takahashi Y 1978 *J. Phys. Soc. Jpn.* **45** 397

[35] Birch F, *Phys. Rev*. 1947 **71** 809

[36] Wu Y, Wu X, Qin S and Yang K 2013 *J. Alloys Compd.* **558** 160

[37] Diop L V B, Isnard O, Arnold Z, Itié J P, Kastil J and Kamarad 2017 *Solid State Comm.* **252** 29